Pergamon

Int. J. Heat Mass Transfer. Vol. 40, No. 7, pp. 1601–1609, 1997

0017–9310/97 $17.00+0.00

PII: S0017–9310(96)00206–2

Hygrostress-multicrack formation and propagation in cylindrical viscoelastic food undergoing heat and moisture transfer processes

TOMOHIRO AKIYAMA,† HONG LIU and KAN-ICHI HAYAKAWA‡

Department of Food Science, New Jersey Agricultural Experiment Station, Cook College, Rutgers University, P.O. Box 231, New Brunswick, NJ 08903, U.S.A.

(*Received* 23 *October* 1995 *and in final form* 30 *May* 1996)

Abstract—Several foods stress-crack during heat and moisture transfer processes without careful process control. Since published simulation studies on stress-cracking were scarce, the present study aimed to develop and validate a model for simulating heat and moisture transfer, hygrostress crack formation and propagation in cylindrical, viscoelastic food. For this, an improved Luikov's model for heat and moisture transfer was used together with the virtual work principle of a viscoelastically deforming body, a critical tensile stress criterion for stress crack formation and a crack-tip-opening-angle criterion for stress crack propagation. Copyright © 1996 Elsevier Science Ltd.

INTRODUCTION

Many food products, without careful process control, undergo structural failure (stress crack formation and propagation) during drying processes, resulting in significant economic loss to food processors. Since structural failure is closely related to stress formation in food resulting from nonuniform shrinkage, several researchers have developed methods for simulating heat and moisture transfer and stress formation, as reviewed in previous publications [1, 2].

According to our literature search, only one published article [1] shows simulation of stress crack propagation in food, although such simulation is useful to drying process optimization. This published article assumed *elastoplastic*, cylindrical food for the model development and used a crack-tip-opening-angle criterion for propagation [3, 4], since it was applicable to multiple crack propagation. The present study was to develop a model for simultaneous heat and moisture transfer and stress crack formation and propagation in *viscoelastic*, cylindrical food since many foods are viscoelastic.

MATHEMATICAL MODEL

Heat and moisture transfer

Simultaneous, transient state heat and moisture transfer in food (deformable solid) is simulated by the following modified Luikov's model [5, 6]

$$\{C_p\rho-\Delta H_v L_k(\rho_s+W\,\partial\rho_s/\partial W)C_T\}\,\partial T/\partial t$$
$$-\Delta H_v L_k(\rho_s+W\,\partial\rho_s/\partial W)C_m\,\partial\phi/\partial t=-\mathrm{div}(\mathbf{J_h}) \quad (1)$$

$$(\rho_s-W\,\partial\rho_s/\partial W)(C_m\,\partial\phi/\partial t+C_T\,\partial T/\partial t)=-\mathrm{div}(\mathbf{J_m}). \quad (2)$$

Fluxes $\mathbf{J_h}$ and $\mathbf{J_m}$ in the above equations are expressed as follows for a homogeneous food.

$$\mathbf{J_h}=-\mathbf{k_t}\cdot\mathrm{grad}(T) \quad (3)$$

$$\mathbf{J_m}=-\mathbf{D_w}\cdot[\rho_s C_m\,\mathrm{grad}(\phi)+\rho_s C_T\,\mathrm{grad}(T)+W\,\mathrm{grad}(\rho_s)]+\mathbf{D_t}\cdot\mathrm{grad}(T). \quad (4)$$

The mass transfer potential ϕ in the above equations was defined as follows [6]:

$$\phi=\begin{cases}\mu_0+RT\ln(a_w) & \text{for } W\leqslant W_m\\ \mu_0[(W-W_m)/(W_m-W^\circ)+1] & \text{for } W\geqslant W_m.\end{cases} \quad (5)$$

Water activity a_w was estimated by the Guggenheim–Anderson–de Bor (GAB) isotherm equation as a function of W and T [7, 8]. The differential dW is related to $d\phi$ and dT as follows.

$$dW=(\partial W/\partial\phi)_T\,d\phi+(\partial W/\partial T)_\phi\,dT$$
$$=C_m\,d\phi+C_T\,dT. \quad (6)$$

The moisture concentration W in equations (1), (2) and (4) was expressed as a function of ϕ and T using equation (5) and GAB equation. The initial and boundary conditions are:

$$\phi=\phi_0 \quad T=T_0 \quad \text{at } t=0 \quad (7)$$

† Current affiliation: Institute of Advanced Materials Processing, Tohoku University, Katahira 2-1-1, Aoba-ku, Sendai 980, Japan.

‡ Author to whom correspondence should be addressed.

NOMENCLATURE

$\mathbf{A}$ deformation–strain matrix defined by equation (18) [m^{-1}]
a_M moisture shift factor
a_T temperature shift factor
a_W water activity
$\mathbf{B}$ matrix product of $\mathbf{A}$ and $\mathbf{N}$
C component of matrix $\mathbf{C}$ when it is appended with subscripts [Pa]
$\mathbf{C}$ mechanical property matrix defined by equation (12)
$\mathbf{C}^s$ 4×4 matrix whose major diagonal elements are $3K$, $3K$, $3K$, and G and whose off diagonal elements are all zeros
C^s component of $\mathbf{C}^s$ when it is appended with subscripts [Pa]
C_m specific mass capacity [kg water (kg dry solid °M)$^{-1}$]
C_T specific temperature coefficient [kg water (kg dry solid K)$^{-1}$]
C_p specific heat [kJ kg^{-1} K^{-1}]
$\mathbf{D}_t$ anisotropic Soret mass diffusivity [kg m^{-1} s^{-1} K^{-1}]
$\mathbf{D}_w$ anisotropic moisture diffusivity [m^2 s^{-1}]
$\mathbf{d}$ nodal displacement vector [m]
$E(t)$ relaxation modulus [Pa]
e_{cf}, e_{cp} random variates of square distribution whose minimum and maximum values are -1 and $+1$, respectively
f_{cf}, f_{cp} empirical constants [Pa kg dry solid (kg water)$^{-1}$; rad kg dry solid (kg water)$^{-1}$]
G shear modulus [Pa]
ΔH_v latent heat of moisture vaporization or condensation [kJ kg^{-1}]
h_m mass transfer coefficient [kg m^{-2} Pa^{-1} s^{-1}]
h_t heat transfer coefficient [W m^2 k^{-1}]
$\mathbf{J}_h$ heat flux [W m^{-2}]
$\mathbf{J}_m$ moisture flux [kg m^{-2} s^{-1}]
j summation index
K bulk modulus [Pa]
$\mathbf{K}$ stiffness matrix defined by equation (24)
$\mathbf{k}_t$ anisotropic thermal conductivity [W m^{-1} K^{-1}]
L cylindrical periodic length. Periodic changes in temperature, moisture and mechanical responses along axial direction of an infinite cylinder assumed [m]
L_g empirical constant in GAB equation
L_k Luikov's phase convergence criterion
$\mathbf{N}$ matrix of shape functions for eight nodes isoparametric element
$\mathbf{n}$ outward normal unit vector [m]
p vapor pressure [Pa]
p_{cf}, p_{cp} empirical constants
p_e equilibrium vapor pressure [Pa]
Q empirical constant in GAB isotherm equation
q_{cf}, q_{cp} empirical constant [Pa; rad]
R gas constant or cylindrical radius [J mol^{-1} K^{-1}; m]
$\mathbf{R}$ force vector defined by equation (23)
r radial direction variable [m]
S_{cf}, S_{cp} empirical constants defined by equations (20) and (22), respectively [m^{-1}]
S_v hygrostress free volumetric shrinkage coefficient
T temperature [K]
t time [s]
$\mathbf{U}$ displacement vector [m]
U element of $\mathbf{U}$ when it is appended with subscript [m]
W moisture content [kg water (kg dry solid)$^{-1}$]
W_{cf}, W_{cp} fixed moisture concentration in empirical equations for estimating critical tensile stress for crack formation and critical tip opening angle for crack propagation, respectively [g water (g dry solid)$^{-1}$]
W_g monolayer moisture value used in GAB isotherm equation [kg water (kg dry solid)$^{-1}$]
W_m moisture content equilibrated to 100% relative humidity [kg water (kg dry solid)$^{-1}$]
W^0 moisture content equilibrated to 0% relative humidity [kg water (kg dry solid)$^{-1}$]
z axial direction variable [m].

Greek symbols

Γ functional defined by equation (16)
Δ finite increment
$\boldsymbol{\varepsilon}$ tensor of total, observed strains, arranged in a single column form
ε element of $\boldsymbol{\varepsilon}$ when it is appended with subscript s
$\boldsymbol{\varepsilon}^s$ tensor of stress free deformation strains arranged in a single column form
ε^s element of $\boldsymbol{\varepsilon}^s$ when it is appended with subscripts
λ reduced time [s]
μ_0 chemical potential of saturated free water [J mol^{-1}]
ξ dummy variable
ρ density of food as initial state [kg m^{-3}]
ρ_s density of porous dried solid [kg m^{-3}]

$\boldsymbol{\sigma}$	stress tensor expressed in a single column form [Pa]
σ	stress component when it is appended with a subscript [Pa]
σ_{cf}	critical tensile stress for crack formation [Pa]
σ_p	tensile principal stress [Pa]
ν	Poisson's ratio
τ	reduced time [s]
ϕ	mass transfer potential [°M]
Ω	crack-tip-opening-angle [rad]
Ω_{cp}	Ω for crack propagation [rad].

Subscripts

a	ambient
c	center
o	initial
e	equilibrium
i,j	dummy subscripts representing, x, y, z, xx, yy, zz, xy, yz, or zx
k,ℓ	dummy subscript representing x, y, or z
m,n	dummy summation indices
s	surface
sa	saturation.

Superscripts

T	transpose
—	average.

$$h_t(T_a-T)-h_m(1-L_k)\,\Delta H_v(p_s-p_a)=\mathbf{J_k}\cdot\mathbf{n} \quad \text{at } r=R \tag{8a}$$

$$h_m(p_s-p_a)=\mathbf{J_m}\cdot\mathbf{n} \quad \text{at } r=R \tag{8b}$$

where $p_i=p_{sa,i}\exp\{(\phi_i-\mu_{o,i})/(RT_i)\}$

$$\text{when } \phi_i\leqslant\mu_o \quad j=s \text{ or } a \tag{8c}$$

$$p_i=p_{sa,i} \quad \text{when } \phi_i>\mu_o \quad i=s \text{ or } a \tag{8d}$$

$$\left.\begin{aligned}\partial T/\partial z=0,\quad \partial\phi/\partial z=0 \quad \text{at } z=\pm L\\ \partial T/\partial r=0,\quad \partial\phi/\partial r=0 \quad \text{at } r=0\end{aligned}\right\} \tag{9}$$

Viscoelastic strain–stress formation

The following shows governing equations expressed in cylindrical coordinates using vectorial presentation of strain and stress tensors.

Constitutive equations.

$$\sigma_i=\int_0^t C_{ij}[\lambda(t)-\lambda(\tau)]\{\partial[\varepsilon_j(\tau)-\varepsilon_j^s(\tau)]/\partial\tau\}\,d\tau. \tag{10}$$

The convolution integration of equation (10) may be represented as:

$$\sigma_i=C_{ij}*(\varepsilon_j-\varepsilon_j^s) \tag{11}$$

where

$$C=\begin{bmatrix}K_p & K_n & K_n & 0\\ K_n & K_p & K_n & 0\\ K_n & K_n & K_p & 0\\ 0 & 0 & 0 & G\end{bmatrix} \tag{12}$$

$$K_p=K+4G/3,\quad K_n=K-2G/3 \tag{13a}$$

$$K=E(t)/[3(1-2\nu)],\quad G=E(t)/[2(1+\nu)] \tag{13b}$$

$$\boldsymbol{\sigma}=\begin{bmatrix}\sigma_r\\ \sigma_z\\ \sigma_\theta\\ \sigma_{rz}\end{bmatrix}\quad \boldsymbol{\varepsilon}=\begin{bmatrix}\varepsilon_r\\ \varepsilon_z\\ \varepsilon_\theta\\ \varepsilon_{rz}\end{bmatrix}\quad \boldsymbol{\varepsilon}^s=\begin{bmatrix}S_v^{1/3}-1\\ S_v^{1/3}-1\\ S_v^{1/3}-1\\ 0\end{bmatrix} \tag{14}$$

$$\lambda(t)=t/\{a_T(T)a_m(W)\}. \tag{15}$$

Note that temperature and moisture dependent viscoelastic properties were estimated through the use of reduced time $\lambda(t)$, a ratio of clock time and product of temperature and moisture shift factors.

Virtual work.

$$\delta\Gamma(\mathbf{U})=\delta\{(1/2)\textstyle\int_v[C_{ij}*\varepsilon_i*\varepsilon_j-C_{ij}^s*\varepsilon_i^s*\varepsilon_j]\,dv\}=0$$

$$:\Gamma(\mathbf{U})=\text{minimum}. \tag{16}$$

Where two terms in the integrant of above equation are convolution integrals.

Strain-displacement.

$$\boldsymbol{\varepsilon}=[\mathbf{A}]\{\mathbf{U}\} \tag{17}$$

$$\mathbf{A}=\begin{bmatrix}\partial/\partial r & 0\\ 0 & \partial/\partial z\\ 1/r & 0\\ \partial/\partial z & \partial/\partial r\end{bmatrix}\quad \mathbf{U}=\begin{bmatrix}U_r\\ U_z\end{bmatrix}. \tag{18}$$

Crack formation and propagation

The tensile, normal stress criterion was used for simulating crack formation since this criterion was applicable to brittle material and used successfully to simulate food drying [1, 2, 9–11].

The normal stress, either tension or compression, becomes locally maximum in the direction of one of three tensorial principal vectors, and the magnitude is equal to the corresponding principal value, positive being tension and negative being compression, and the three principal vectors being orthogonal to each

other. The principal vectors and principal values were estimated after rearranging the vectorially expressed stresses, equation (14), into a two-dimensional, tensorial form.

According to the critical tensile stress criterion, a crack is formed at a location where the applicable tension principal stress σ_p satisfies the following condition [1]:

$$\sigma_p \geqslant \sigma_{cf}$$

where

$$\sigma_{cf} = \begin{cases} (1+S_{cf}z_0)q_{cf} & W \geqslant W_{cf} \\ (1+S_{cf}z_0)\{f_{cf}(W-W_{cf})+q_{cf}\} & W \leqslant W_{cf} \end{cases} \quad (19)$$

where

$$S_{cf} = e_{cf}p_{cf}/z_0, \quad f_{cf} < 0 \quad \text{and } q_{cf} > 0. \quad (20)$$

Equation (19) assumes z-directional random variation in σ_{cf} within $\pm p_{cf}$ through consideration of extrusion processes (variation around q_{cf} when $W > W_{cf}$ and around $f_{cf}(W-W_{cf})+q_{cf}$ when $W < W_{cf}$).

Upon crack formation, a crack propagates when the opening angle of a crack tip, Ω, satisfies the following condition [1]:

$$\Omega \geqslant \Omega_{cp}$$

where

$$\Omega_{cp} = \begin{cases} (1+S_{cp}z_0)\{f_{cp}(W-W_{cp})+q_{cp}\} & W \geqslant W_{cp} \\ (1+S_{cp}z_0)q_{cp} & W \leqslant W_{cp} \end{cases} \quad (21)$$

where

$$S_{cp} = e_{cp}p_{cp}/z_0, \quad f_{cp} > 0 \quad \text{and } q_{cp} > 0. \quad (22)$$

Equation (21) assumed random variation of Ω_{cp} similar to σ_{cf}.

When a stress crack formed or propagated, stresses orthogonal to the newly formed crack-gap faces relaxed to nil. Additionally, the lower limits of the convolution integrals, equation (10), for these relaxed stresses were shifted to the onset of the crack formation or propagation from a zero time. It was assumed that a micro-void space created by each crack formation/propagation was filled with air whose temperature and humidity are equilibrated to those along crack-surface.

Numerical solution algorithm

All governing equations were solved by applying a Galerkin finite element method. For this application, a solution domain was subdivided into curved side isoparametric elements, 8 nodes per element.

The method used for solving the heat and moisture transfer equations was similar to the one used previously in ref. [1]. Viscoelastic hygrostrain-stresses were estimated through an approach similar to previous work [2]. When the finite element method was applied, equation (16) became:

$$\mathbf{K} * \mathbf{d} = \mathbf{R} \quad (23)$$

where

$$\mathbf{K} = \sum_{e=1}^{n_e} \int_{ve} \mathbf{B}^T \cdot \mathbf{C} \cdot \mathbf{B} \, dv \quad (24)$$

$$\mathbf{R} = \sum_{e=1}^{n_e} \int_{v_e} \mathbf{B}^T \mathbf{C}^s * \boldsymbol{\varepsilon}^s \, dv \quad (25)$$

$$\mathbf{B} = \mathbf{A} \cdot \mathbf{N}. \quad (26)$$

The displacement increment, $\Delta\mathbf{U}$, at any location within an element was estimated form nodal displacement increment, $\Delta\mathbf{d}$ by:

$$\Delta\mathbf{U} = \mathbf{N} \cdot \Delta\mathbf{d}. \quad (27)$$

The strain increment, $\Delta\boldsymbol{\varepsilon}$, at any location in an element was estimated from $\Delta\mathbf{U}$ by:

$$\Delta\boldsymbol{\varepsilon} = \mathbf{A} \cdot \Delta\mathbf{U} = \mathbf{A} \cdot \mathbf{N} \cdot \Delta\mathbf{d} = \mathbf{B} \cdot \Delta\mathbf{d}. \quad (28)$$

Using the convolution integral definition equation (23) became:

$$\int_{\xi=0}^{t} \mathbf{K}[\lambda(t) - \lambda(\xi)](\partial d(\xi)/\partial\xi) \, d\xi = R(t). \quad (29)$$

The numerical integration of equation (29) produced:

$$\sum_{m=0}^{n+1} \mathbf{K}[\lambda(t_{n+1}) - \lambda(t_m)] \, \Delta\mathbf{d}(t_m) = \mathbf{R}(t_{n+1}). \quad (30)$$

Using equation (30), the nodal displacement increment, $\Delta\mathbf{d}(t_{n+1})$, at the next time step was estimated.

$$\mathbf{K}(0) \, \Delta\mathbf{d}(t_{n+1}) = \mathbf{R}(t_{n+1}) - \sum_{m=0}^{n} \mathbf{K}[\lambda(t_{n+1}) - \lambda(t_m)] \, \Delta\mathbf{d}(t_m). \quad (31)$$

Finally, the stresses at the next time step, t_{n+1}, was estimated using equation (10).

$$\sigma(t_{n+1}) = \sum_{m-0}^{n+1} \mathbf{C}[\lambda(t_{n+1}) - \lambda(t_m)]\mathbf{B} \, \Delta\mathbf{d}(t_m) - \sum_{m=0}^{n+1} \mathbf{C}[\lambda(t_{n+1}) - \lambda(t_m)] \cdot \Delta\boldsymbol{\varepsilon}^s(t_{n+1}). \quad (32)$$

Since $\mathbf{B}$, $\mathbf{C}$ and $\mathbf{K}$ were temperature and moisture dependent, nodal temperature and moisture concentration histories were required to estimate $\boldsymbol{\sigma}(t_{n+1})$. Nodal displacements were estimated by:

$$\mathbf{d}(t_{n+1}) = \mathbf{d}(t_n) + \Delta\mathbf{d}(t_{n+1}). \quad (33)$$

It should be noted that equations (31) and (32) include the summation of many terms, especially in a late stage of a drying or hydrating process, resulting in accumulated truncation errors and lengthy computer time. Double precision computation was employed to

control truncation errors. Computer time was reduced by estimating nodal displacements and stresses at every other time increment for heat and moisture transfer estimation since results obtained were virtually identical to those estimated at each time increment.

According to our previous work [1, 2, 11], a stress crack was formed orthogonally to the critical stress. Preliminary simulation results showed that the magnitudes of principal tensile stresses in the axial direction were greater than those in the radial direction. Therefore, stress cracks would form and propagate in the radial direction (orthogonal to the axial principal stresses of critical levels).

The above observation was used for finite element discretization of a solution domain, axially bisected face. Algorithms for estimating multiple stress crack formation and propagation were similar to those presented in a previous paper [1].

EXPERIMENTAL VALIDATION

Drying experiments were conducted for model validation using cylindrical samples made from hydrated high amylose starch powders, 0.40 g moisture/g dry matter (Hylon 7, National Starch and Chemical Co., Springfield, NJ). The initial dimensions of each sample were 10 mm in diameter by 140 mm in length. Two samples had thermocouples installed in their geometrical centers to monitor temperatures during drying. Several other samples were used to monitor weight changes or stress-crack formation and propagation.

Each sample was prepared using two identical molds made of plaster, each with an axial bisection of a cylinder. The molds were filled with starch hydrate and placed together to form a solid cylinder by compression. To make a sample with an installed thermocouple (copper–constantan 36 gauge wires), a junction was placed at the axial center before placing the molds together, the copper and constantan wires laying on the cylindrical axis and coming out separately from the cylinder through the two opposing ends.

The samples were dried in a forced air, pilot plant dryer (Sargent & Sons Corp., Graniteville, MA) at a flow rate of 2 ms^{-1} at 332°K and relative humidity of the air 11%. Sample temperatures were recorded during drying by a digital data logger. The three samples without installed thermocouples were taken out from the dryer through a sampling port, to measure weights by an analytical balance (Model PE160, Mettler Instrument Co., Hightstown, NJ). The time required for weight measurement was about 20 s. This did not influence sample weight change according to a preliminary experiment (taking samples out at different time intervals). Upon completion of drying, sample dry matter was determined using a vacuum oven method [12]. Changes in sample moisture were estimated from differences between current weight and dry matter weight. Stress crack formation and propagation within samples were observed with those removed from the dryer at 180, 360 and 1800 s of drying. Each sample was carefully bisected along its central axis without disturbing the internal structure in order to photograph its bisected face (different samples for different drying times). Heat and moisture transfer and mechanical properties were obtained from previously published papers, Table 1 [1, 2, 6].

A separate experiment was conducted as described above to determine h_m and h_q values. This determination was based on minimizing the sum of squares of differences between observed and predicted central temperatures or average moisture concentrations assuming different sets of h_m and h_q values.

Figure 1 shows observed and predicted temperature and moisture histories of the samples (averages of three measurements for W/W_0 and of two T_c measurements). There is good agreement between the observed and predicted results.

Figure 2 shows photographs of the bisected face at the mid-length section of samples taken at 180, 360 and 1800 s of drying. The exposed surface and central axis positions are shown in the figure.

At 180 s of drying, several small cracks were visible, mostly extending from the surface positions. Dark patches in the interior were shadows of the irregular face. The lengths of surface cracks were about 5–15% of the sample radius. Cracks extending from the surface became wider and crack lengths increased to 20–30% of the radius when drying progressed to 360 s. Further increases in crack width and length (35–70% of the diameter) are apparent from the picture at 1800 s.

Figure 3 shows simulation results on principal stress distributions and stress cracks formed on the one half of a bisected face at 36, 180, 360 and 1800 s of drying. The lower horizontal line, the abscissa, of each drying time figure is the central axis and the upper line the

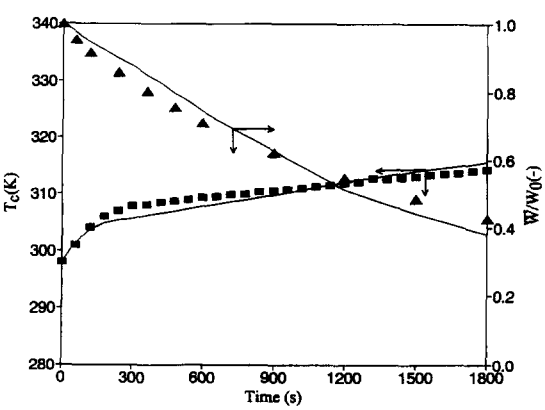

Fig. 1. Central temperature and average moisture concentration histories of cylinder made of hydrated high amylose starch powders (diameter 10 mm, length 140 mm). Solid lines are estimated results. Solid triangles are observed ratios of average moisture and initial moisture concentrations; solid squares are observed central temperatures.

Table 1. Drying conditions and physical mechanical properties used for the simulation

Drying conditions	
Ambient temperature (T_a) [K]	332
Initial temperature (T_0) [K]	298
Initial moisture content (W_0) [kg-water (kg solid)$^{-1}$]	0.40
Initial density (ρ_{s0}) [kg m^{-3}]	0.603×10^3
Relative humidity in air (RH)	0.11
Physical properties	
Heat transfer coefficient (h_t) [W m^{-2} K^{-1}]	23.2
Mass transfer coefficient (h_m) [m s^{-1}]	9.7×10^{-6}
Volumetric shrinkage coefficient (S_v)	$1.734/[1.734 + W_0 - 0.2)]$ for $W \leqslant 0.2$ $[1.734 + (W - 0.2)]/[1.734 + W_0 - 0.2)]$ for $W \geqslant 0.2$
Moisture diffusivity (D_w) [m^2 s^{-1}] Lagrangian interpolation polynomial fitted to experimental data [13]	
Soret mass diffusivity (D_t) [kg m^{-1} s^{-1} K^{-1}]	$0.001\ D_w$
Thermal conductivity (k_t) [W m^{-1} K^{-1}]	$0.03332 + 1.16 \times 10^{-3} T + 0.058 W/(1 + W)$
Luikov's phase conversion criteria (L_k)	$1 - W/W_0$
Specific heat (C_p) [J kg^{-1} K^{-1}]	$5203.3 - 12.1T + 1730W/(1 + W)$
GAB equation	$W_e = W_g Q L_g a_w / [(1 - L_g a_w)(1 - L_g a_w + Q L_g a_w)]$ $W_g = 7.259 \times 10^2 \exp(162.6/T)$ $Q = 7.198 \times 10^4 \exp(3021/T)$ $L_g = 0.370 \exp(142.1/T)$
C_m, C_T	$\partial W/\partial \phi$ and $\partial W/\partial T$ estimated after substitution of GAB equation to equation (5), noting the μ_0 being temperature dependent
Mechanical properties	
Relaxation modulus of starch ($E(t)$) [MPa]	$50\{1.31 \times 10^2 + 2.00 \times 10^2 \exp(-t/(3.50 \times 10^2 \alpha_T(T)\alpha_M(W))) + 82.7 \exp(-t/(1.43 \times 10^2 \alpha_t(T)\alpha_M(W)))\}$
Temperature shift factor ($\alpha_T(T)$)	$\exp\{-0.02(T - 298) - 6.75 \times 10^{-4}(T - 298)\}$
Moisture shift factor ($\alpha_M(W)$)	$\exp\{-170(W - 0.28)\}$
Poisson's ratio (ν) [−]	0.3
Critical stress (σ_{cf} [kPa])	$(1 + S_{cf} z_0)(147.65 - 4850W)$ for $W < 0.289$ $(1 + S_{cf} z_0)70$ for $W > 0.289$ $P_{cf} = 0.04$
Critical crack tip opening angle Ω_{cp} [rad]	$(\pi/180)\ (1 + S_{cp} z_0)\ 1.6$ for $W < 0.289$ $(\pi/180)\ (1 + S_{cp} z_0)\ [1.6 + 2.97(W - 0.289)]$ for $W > 0.289$ $P_{cp} = 0.04$

exposed surface. The ordinate of each figure is the radial distance measured from the central axis. Each figure shows two principal stresses acting at each selected location on the bisected surface together with stress cracks. Each of the two stresses, orthogonal to each other, is represented by a solid or broken line segment; solid and broken lines being tension and compression, respectively. A bar is missing when a stress is too small to show. Stresses are applicable at the point of intersection of two bars when both are shown or at the mid-point of a bar when one of a pair is missing. One remaining principal stress acted at each location on a plane orthogonal to the bisected face; it was not shown in the figure since the mag-

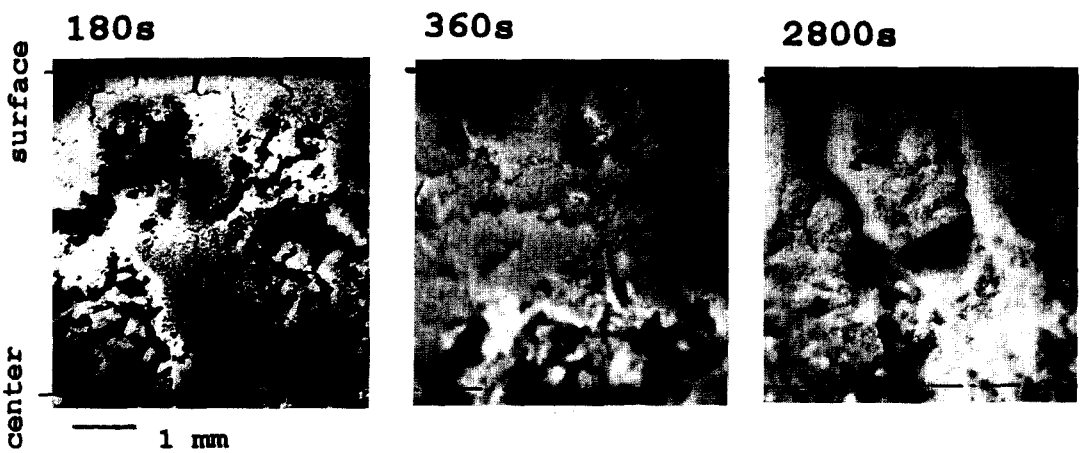

Fig. 2. Photographs of cracks on axially bisected faces of samples at 180, 360 and 1800 s of drying.

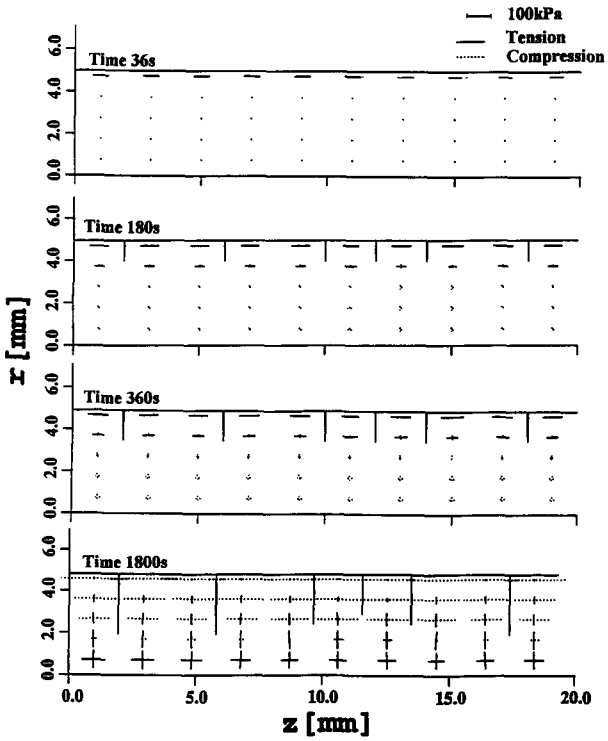

Fig. 3. Estimated hygrostresses at selected locations and stress cracks on axially bisected faces of a starch hydrate sample at 180, 360 and 1800 s of drying. The ordinate and abscissa of each subfigure are the radial and axial coordinates, respectively. The line parallel to the abscissa is the exposed surface. Vertical line segments extending from the exposed surface line at 180, 360 and 1800 s are cracks. Solid or broken bars, parallel or orthogonal to the exposed surface line are principal stresses.

nitude was less than those shown. Vertical solid bars extending from the exposed surface toward the central axis are cracks. The volumetric shrinkage of the sample is apparent from changes in the surface line position and sample length.

At 36 s of drying, there were axial, tensile stresses in a surface zone. The maximum tensile stress in this zone was about 65 kPa, below the critical stress for crack formation at the moisture level of this zone. Radial stresses are too small to show in the figure (less than 0.05 kPa).

There were cracks extending from the surface to the interior at 180 s. Their sizes were about 20% of the cylindrical radius. Axial tensile stresses formed in the surface zone were about 75 kPa, greater than those formed at 36 s. There were interesting changes in stress magnitudes along the sample radius. At about three-quarters of the cylindrical radius ($r = 0.75\ R$), the axial, tensile stresses decreased to about one half of the stresses on the surface. Small compressional stresses, barely recognizable in the figure, formed in the radial direction at the same location. When r was reduced to about 0.6 R, small compressional stresses were formed in both radial and axial directions. The magnitudes of compressional stresses increased slightly with further reduction in r. At 360 s, crack sizes increased to about 30% of the cylindrical radius. Stress magnitudes were slightly greater than those at 180 s. Tension to compression conversion along the radius was similar to one observed at 180 s. At 1800 s, crack sizes increased to 40–60% of the radius. Additionally, surface stresses changed from tension to compression and interior stresses from compression to tension. This was due to the fact that there was no further shrinkage in the surface zone, since $W < 0.2$ kg moisture/kg dry solid (0.2 being a critical W of S_v) or $W/W_0 < 0.5$ in this zone, while an interior region close to the central axis continued to shrink since $W/W_0 > 0.5$. The stress conversion was due to a mechanical interaction between the surface and interior zones.

The estimated crack sizes agreed well with those observed experimentally. The observed crack sizes were 5–15, 20–30, and 35–70% of the sample radius at 108, 360 and 1800 s of drying, respectively. Whereas, the estimated crack sizes were 20, 30, and 40–60% at the same respective drying times.

Figure 4 shows simulated temperature distribution in the bisected face at the four different drying times corresponding to the previous figure; figures next to isothermal lines, dotted lines, are temperatures. The temperature distribution became almost uniform at 180 s of drying, 0.4C° maximum temperature difference. Isothermal lines were parallel to the exposed surface at 36 s. However, they became highly irregular when stress cracks were formed due to locally enhanced heat transfer by cracks. Figure 5 shows moisture distributions. Figures given next to iso-concentration lines are ratios of current and initial moist-

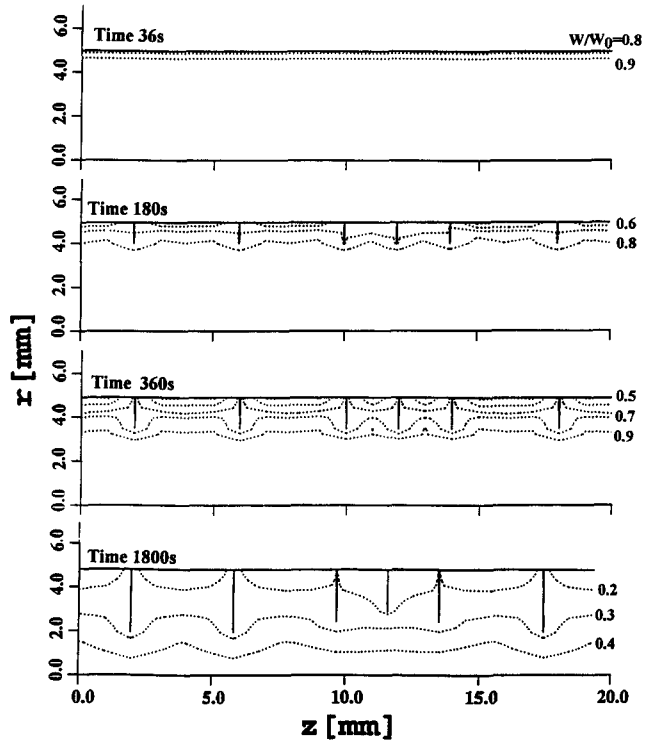

Fig. 4. Estimated temperature distributions on axially bisected faces of a starch hydrate sample at 36, 180, 360 and 1800 s of drying. Dotted lines are isotherms. Figures by these lines are temperatures.

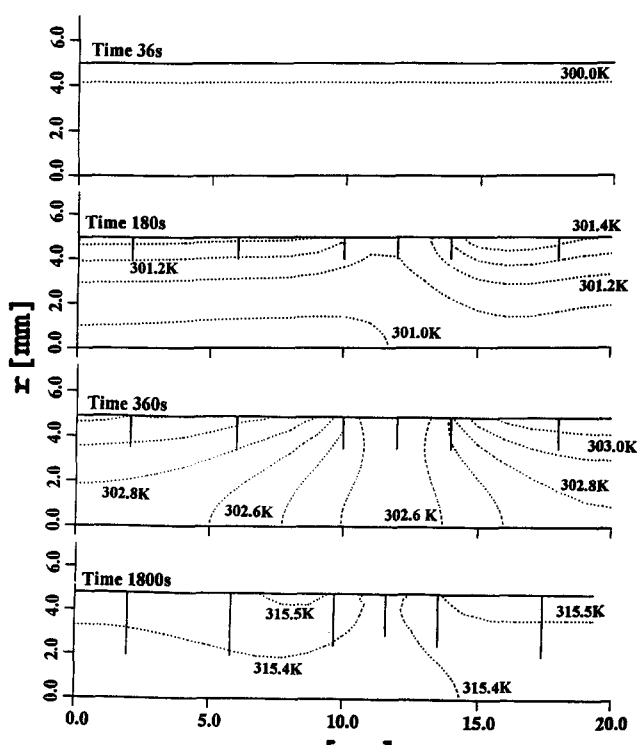

Fig. 5. Estimated moisture concentration distribution on axially bisected faces of a starch hydrate sample at 36, 180, 360 and 1800 s of drying. Dotted lines are isoconcentration lines. Figures by these lines are ratios of current and initial moisture concentrations.

ure concentrations. As with temperature distribution, moisture distributions became irregular after stress crack formation. There were considerable concentration gradients at 1800 s, since the moisture transfer was much slower than the heat transfer. Therefore, tensile stresses of considerable magnitudes existed at this time, as shown in Fig. 3. The same stresses are likely to exist in a food product at the end of drying, especially when it is dried quickly for a short time. These stresses may cause structural damage to the product when it is handled improperly. The stresses relax to nil when moisture distribution becomes gradually uniform through self-diffusion.

Acknowledgements—This material is based on work supported in part by: USDA NRI Competitive Grants Program (value added program) award no. 94-37500-0683, the Center for Advanced Food Technology, a New Jersey Commission on Science and Technology Center, NSF Advanced Computing Resources grant administered at the Pittsburgh Supercomputing Center, New Jersey State Fund, U.S. Hatch Act Fund, Rutgers University computing service center time, New Jersey Agricultural Experiment Station Publication nos D10973-1-96 and D10535-1-96.

REFERENCES

1. Izumi, M. and Hayakawa, K., Heat and moisture transfer and hygrostress crack formation and propagation in cylindrical, elastoplastic food. *International Journal of Heat and Mass Transfer*, 1995, **38,** 1033–1041.
2. Itaya, Y., Kobayashi, T. and Hayakawa, K., Three dimensional heat and moisture transfer with microelastic strain–stress formation in composite food during drying. *International Journal of Heat and Mass Transfer*, 1995, **38,** 1173–1185.
3. Newman, J. C. Jr, An elastic–plastic finite element analysis of crack initiation, stable crack growth, and instability. *Fracture Mechanics Fifteenth Symposium*, American Society for Testing Materials, ASTM STP-833, 1984, pp. 93–117.
4. Shivakumar, K. N. and Crews, J. H., Jr, Energy dissipation associated with crack extension in an elastic–plastic material. *Engineering and Fracture Mechanics*, 1987, **26,** 319–330.
5. Furuta, T. and Hayakawa, K., Heat and moisture transfer with thermodynamically interactive fluxes and volumetric changes—I. Mathematical model development and numerical solution. *Transactions of the ASAE*, 1992, **35,** 1537–1546.
6. Sakai, N. and Hayakawa, K., Two dimensional simultaneous heat and moisture transfer in composite food. *Journal of Food Science*, 1992, **57,** 475–480.
7. Lamauro, C. J., Bakshi, A. S. and Labuza, T. B., Evaluation of food moisture sorption isotherm equations. Part I. Fruit and vegetable products. *Lebensm. -Wiss. u. Technol.* 1985, **18,** 111–117.
8. Lamauro, C. J., Bakshi, A. S. and Labuza, T. B., Evaluation of food moisture sorption isotherm equations. Part II, Milk, coffee, tea, nuts, oil seeds, spices, and starch foods. *Lebensm. -Wiss. u. -Technol.* 1985, **18,** 118–124.
9. Litchfield, J. B. and Okos, M. R., Prediction of corn kernel stress and breakage induced by drying, tempering and cooling. *Transactions of the ASAE*, 1988, **31,** 585–594.
10. Haghighi and Serglind, L. J., Failure of biomaterials subjected to temperature and moisture gradients using the finite element method: I—thermohydro-viscoelasticity. *Transactions of the ASAE*, 1988, **31,** 930–937.
11. Tsukada, T., Sakai, N. and Hayakawa, K., Computerized model for strain–stress analysis of food undergoing a simultaneous heat and mass transfer process. *Journal of Food Science*, 1991, **56,** 1436–1445.
12. Anonymous. *Official Method of Analysis*, 12th edn. Association of Official Analytical Chemicals, Washington, DC, 1980.
13. Marousis, S. N., Karathanos, V. T. and Saravacos, G. D., Effect of sugars on the water diffusivity in hydrated granular starches. *Journal of Food Science*, 1989, **54,** 1496–1552.